Physics of Plasmas

RESEARCH ARTICLE | AUGUST 01 2024

Compact Compton γ-ray source from a spatiotemporal-modulated pulse scattering a high-energy electron beam

Q. Yu ; Y. J. Gu ; Y. Zhang ; Q. Kong ; S. Kawata

Phys. Plasmas 31, 083101 (2024)
https://doi.org/10.1063/5.0211695

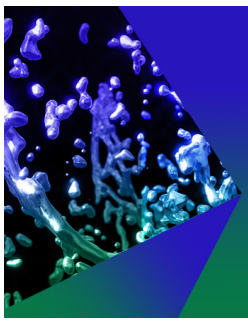

Compact Compton γ-ray source from a spatiotemporal-modulated pulse scattering a high-energy electron beam

Cite as: Phys. Plasmas **31**, 083101 (2024); doi: 10.1063/5.0211695
Submitted: 1 April 2024 · Accepted: 6 July 2024 ·
Published Online: 1 August 2024

Q. Yu,[1,a)] Y. J. Gu,[2,3] Y. Zhang,[1,a)] Q. Kong,[4,a)] and S. Kawata[5]

AFFILIATIONS

[1]School of Mechanical Engineering and Rail Transit, Changzhou University, Changzhou 213164, China
[2]Institute of Laser Engineering, Osaka University, Suita, Osaka 565-0871, Japan
[3]Institute of Physics of the ASCR, ELI-Beamlines, Na Slovance 2, 18221 Prague, Czech Republic
[4]Key Laboratory of Nuclear Physics and Ion-beam Application (MOE), Institute of Modern Physics, Department of Nuclear Science and Technology, Fudan University, Shanghai 200433, China
[5]Graduate School of Engineering, Utsunomiya University, Utsunomiya 321-8585, Japan

[a)]**Authors to whom correspondence should be addressed:** qqyu@cczu.edu.cn; zhangyi1976@126.com; and qkong@fudan.edu.cn

ABSTRACT

A novel plasma mirror is proposed for realizing all-optical Compton scattering, and its performance is compared with that of planar and concave plasma mirrors. Compared to a planar mirror, a concave mirror augments the radiation energy, but it decreases the collimation of the emitted photon beam. With the aid of the increased pulse length of the reflected laser, our proposed plasma mirror boosts the radiation energy and simultaneously improving the collimation of the emitted radiation. The pulse length and radius of the reflected laser can be controlled by adjusting the parameters of the proposed plasma mirror. The dependences of the pulse length and radius on the mirror parameters have been demonstrated. The impact of non-ideal conditions encountered in real experiments on the proposed mechanism has been discussed, which precisely demonstrates the robustness of the proposed mechanism. Additionally, the required gas density for a wakefield accelerator is derived to achieve optimal scattering under the given plasma mirror configurations.

I. INTRODUCTION

High-quality electron beams have been realized by exploiting high-power lasers and advanced plasma-based accelerator technologies.[1–9] They can be regarded as compact particle accelerators that can be used to drive ultra-compact light sources, yielding a broad spectrum of electromagnetic radiation ranging from THz to x-ray or γ-ray regions. These light sources have excellent applications in numerous fields, including phase contrast imaging,[10–12] radiosurgery,[13] lithography,[14] nuclear resonance fluorescence,[15–17] transmutation of nuclear wastes,[18,19] and generation of medical isotopes.[20–23] Based on the laser and plasma parameters, different regimes can be realized, contributing to the generation of high-quality multi-MeV photon beams. These beams include the betatron radiation produced in a laser wakefield accelerator (LWFA) with under-dense plasmas,[24] synchrotron radiation in laser–solid interactions,[25] bremsstrahlung emission by laser-accelerated fast electrons interacting with high-Z atoms,[26] Compton scattering (CS), or Thomson scattering,[27–30] and in-flight positron annihilation.[31] Recently, all-optical controllable CS or Thomson scattering sources have been widely explored,[29,32,33] aided by routine generation of laser-driven GeV electron beams[5,34–37] in laboratories, thus facilitating the realization of all-optical Compton/Thomson sources.

A CS source bombards a bunch of relativistic electrons with an intense laser pulse. The electrons traveling in the electromagnetic field oscillate and emit synchrotron-like radiation, which is commonly referred to as CS when the quantum effect is considered. The all-optical CS concept has been widely discussed theoretically[38–43] and has been demonstrated in proof-of-principle experiments.[44–46] The entirely optical realization of CS typically requires two counterpropagating relativistic laser pulses:[33,43,47,48] one to evoke an LWFA and the other to scatter the wakefield-accelerated electrons. This leads to two stringent requirements for the experiments: the two counterpropagating laser pulses need to be spatially aligned and temporally

synchronized. To meet these requirements, an alternative approach[29,40,49–53] has been proposed, wherein a planar plasma mirror (PPM) is placed behind the plasma-based accelerator. After the acceleration of the electrons, the PPM reflects the incident laser, which causes it to automatically overlap with the subsequent accelerated beam, thereby achieving all-optical CS. Since this single-pulse CS scheme employs only one laser pulse, the temporal synchronization and spatial alignment of two counterpropagating ultra-short pulses can be disregarded. Thus, this approach can easily be experimentally implemented. Through this single-pulse CS scheme, numerous researchers have successfully generated highly energetic x-ray/γ-ray beams in both experiments[50,51,54,55] and simulations.[29,53,56] Harvey *et al.*[30] comprehensively investigated the effect of the laser profile on scattering and provided a detailed explanation about the dependence of scattering on various laser parameters.

In the aforementioned PPM-based CS mechanism, the emitted photon energy[57,58] is limited by the LWFA driving laser intensity, which is generally small owing to the focusing condition limitations,[59–62] namely, $17\left(\frac{n_c}{n_e}\right)\mathrm{GW} < \mathrm{P} < \frac{n_e R^4}{n_c \lambda^4}$. Here, n_e and n_c are the plasma and critical densities, respectively; λ is the laser wavelength; and P is the laser power. Furthermore, the radius of the scattering laser is usually considerably larger than that of the scattered electron beam, denoting that only the near-axis portion of the laser energy partakes in CS, which significantly reduces the CS efficiency and utilization of the laser. To address these two issues, researchers[29,63–65] have proposed the use of a concave focusing plasma mirror instead of a PPM. For instance, Feng *et al.*[29] successfully fabricated intense γ-rays by employing a focusing plasma mirror to refocus the reflected laser pulse on the LWFA electrons. However, owing to the increase in the transverse field strength of the scattering pulse, the collimation and emittance of the radiation deteriorated. The concave focusing plasma mirror also significantly shortened the effective pulse length of the reflected laser. Nevertheless, as stated in Ref. 30, this parameter is crucial in CS as it affects the scattering time and consequently affects the energy of the radiated photons and laser utilization. Moreover, the negative impact of the reduction in the effective pulse length could neutralize or even overcome the positive effects of the laser intensity enhancement, discussed in Ref. 30.

This study employs an exponential convex focusing plasma mirror (E-FPM) instead of a PPM [or a parabolic concave focusing plasma mirror (P-FPM)] in a PPM-based (or P-FPM-based) CS mechanism (Fig. 1). This particular shape is employed for the mirror because the optical path analysis showed that this shape can longitudinally extend the pulse length of the reflected laser while transversely focusing the reflected laser to increase the laser intensity. This design has the advantages of a P-FPM without its disadvantages. The base of E-FPM is designed to be planar to effectively modulate the reflected laser radius and ensure that it can fully cover the scattered electron beam transversely at the focal point. This is another advantage of E-FPM over P-FPM, as ultra-tight focusing, when using a P-FPM to reflect the laser, can sometimes yield too small a radius of the reflected laser to fully cover the colliding electron beam transversely at the focal spot.

Section II presents a comparison of the effects of PPM, P-FPM, and E-FPM on the CS process and quality of the radiated rays. Section III verifies the promoting effect of the extended pulse length afforded by E-FPM on the quality improvement of the emitted photon beam. Section IV discusses the impacts of various adverse experimental factors on the three scattering schemes. Section V investigates the impact of E-FPM on the reflected laser profile and the scattering effect. Section VI theoretically presents the LWFA density required for realizing high-efficiency laser–electron scattering, with the relevant technical details presented in Appendix. Section VII illustrates the conclusions.

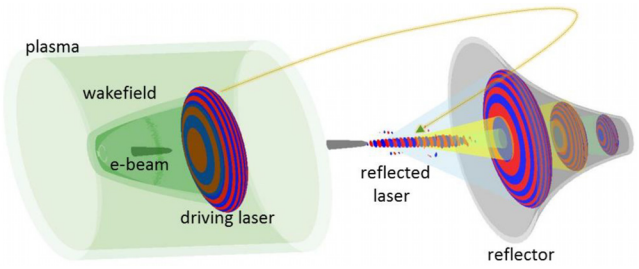

FIG. 1. Schematic of the single-pulse CS based on an exponential focusing reflector and plasma wakefield.

II. COMPARISON OF SINGLE-PULSE CS BASED ON PPM, P-FPM, AND E-FPM

A. Simulation setup

Figure 2 illustrates the schematic of the single-pulse CS scheme based on an LWFA and plasma mirrors. A relativistic laser propagates through an under-dense plasma, evoking a wakefield. The wakefield captures and accelerates the background electrons, and the acceleration ends when the electrons reach the dephasing point. Upon reaching the plasma mirror placed behind the gas target, the driving laser is reflected by the plasma mirror, and the reflected laser reverses its propagation direction and naturally overlaps with the wakefield-accelerated forward-propagating electron beam, thus realizing CS and affording a high-quality light source. Three single-pulse CS processes based on PPM, P-FPM, and E-FPM were investigated via theoretical analyses and numerical simulations. To save simulation resources, the wakefield acceleration process was ignored, which has been already thoroughly researched in numerous studies.[2–4,66–68]

Simulations were performed based on the Particle-in-Cell code VLPL, which represents Virtual Laser Plasma Lab.[69] Unless stated otherwise, the same simulation parameters were employed in all the three cases. The driving pulse was a linearly polarized Gaussian laser pulse with a wavelength (λ) of 1 μm, radius (R) of 10 μm, intensity (a_0) of 1, and pulse duration (L) of 30 λ. The dimensions of the simulation box along and perpendicular to the laser propagation direction were $101\lambda \times 70\lambda$, with a corresponding resolution of $0.03\lambda \times 0.1\lambda$. The wakefield-accelerated energetic electron beam was a preformed $0.01n_c$ electron beam measuring $7\lambda \times 2\lambda$ along and perpendicular to the laser propagation direction. The electron beam propagated from the left to the right with a peak energy of 0.5 GeV and an energy spread of 5%. Four macroparticles were present in each cell for the electron beam. With regard to the plasma mirrors, each cell comprised eight macroparticles and the mass ratio of electrons to ions was 1/1836. The radius and thickness of the plasma mirrors were 35λ and 5λ, respectively, with a density of $5n_c$. The left panel of Fig. 3 depicts the inner surface outlines of the plasma mirrors, which are described as

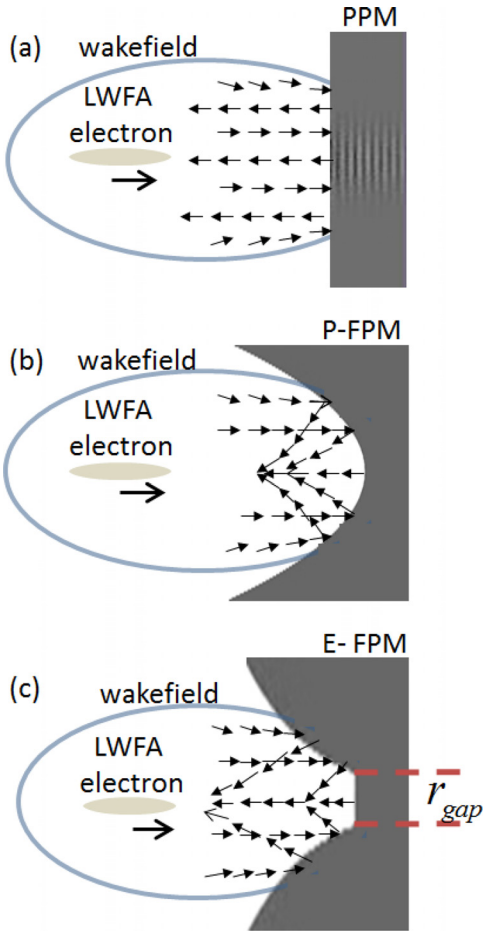

FIG. 2. Schematic of a single-pulse CS based on an LWFA and (a) PPM, (b) P-FPM, and (c) E-FPM. The arrows indicate the propagation directions of the laser photons before and after the reflection.

$$|y| = \begin{cases} x = x_0, & \text{for PPM} \\ \sqrt{k_1(x_1 - x)}, & \text{for P-FPM} \\ e^{k_2(c_0 - x)} - y_0, & x < x_1 \text{ for E-FPM} \end{cases} \quad (1)$$

with $x_0 = 50\lambda$, $x_1 = 86\lambda$, $y_0 = 0$, $k_1 = 12.5$, $k_2 \approx 0.06$, and $c_0 = 101\lambda$. Specifically, k_1 is a coefficient that determines the focal length (f) and curvature change of a parabola through $f = \frac{k_1}{4}$. The larger k_1 is, the greater is the change in the parabolic function; conversely, the smaller k_1 is, the more gradual is the change. In other words, k_1 determines the focal length, aperture size, and curvature change of the parabolic mirror, directly influencing the geometric shape and optical properties of the mirror. k_2 is another coefficient whose magnitude affects the rate of curvature change in an exponential function. The larger k_2 is, the more dramatic is the change in the exponential function; conversely, the smaller k_2 is, the more gradual is the change. k_2 governs the geometric structure and optical properties of an exponential mirror by influencing its aperture size and curvature change. The longitudinal distances between the electron beam mass center and laser center were 26.5λ, 6λ, and 32.5λ for the PPM, P-FPM, and E-FPM cases, respectively. The employed delay distances between the electron beam mass center and laser center in all the three cases guaranteed that the electrons scattered the lasers at the focal points.

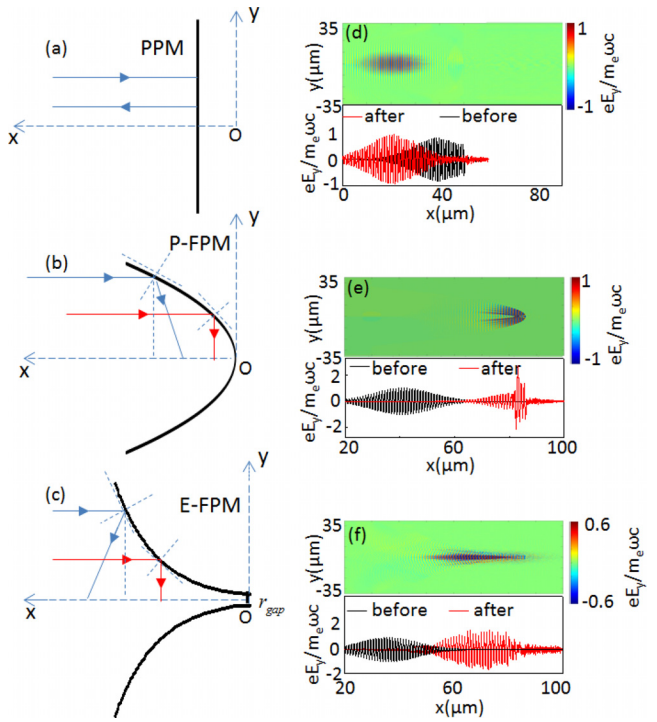

FIG. 3. Laser beam path diagrams after reflection by (a) PPM, (b) P-FPM, and (c) E-FPM. (d)–(f) Corresponding profiles of the laser beams reflected by the three plasma mirrors and corresponding transverse electric field distributions of the reflected lasers along $y = 0$ before and after reflection.

B. Simulation results and discussion

The optical path diagrams in the left panel of Fig. 3 show that PPM barely influences the reflected laser pulse length, P-FPM significantly decreases the reflected laser pulse length, and E-FPM exhibits an extension effect for the reflected laser pulse length. The simulated laser profiles reflected by PPM, P-FPM, and E-FPM (right panel of Fig. 3) verify the theoretical predictions. Based on the theoretical analyses, the pulse lengths of the reflected lasers (L_{ref}) are

$$L_{ref} \approx \begin{cases} L, & \text{for PPM} \\ 0, & \text{for P} - \text{FP} \\ \frac{lnR}{k_2} + \mathrm{R} \cdot \tan\left(2\theta_2 - \frac{\pi}{2}\right), & \text{for E} - \text{FPM}, \end{cases} \quad (2)$$

where $\theta_2 = \arctan(k_2 \cdot R)$. The simulation results approximately matched the theoretical predictions for all the three plasma mirrors, especially in the E-FPM case, where the simulated L_{ref} of approximately 30λ closely agreed with the theoretical result of 33λ.

Furthermore, P-FPM and E-FPM were capable of refocusing the reflected pulse. Depending on the refocusing effect, P-FPM and E-FPM increased the reflected a_0 to approximately 2.9 and 2.0, respectively, from the original value of 1.0. The reflected a_0 value in the E-FPM case was lower than that in the P-FPM case. This was because compared to the latter, the L_{ref} extension effect in the former weakened the focusing effect.

Compared to P-FPM, which caused the reflected pulse to rapidly diverge after the focal spot, E-FPM maintained the focusing profile of the reflected pulse for more than $25T_0$ (T_0 being the laser period), as shown in Fig. 4. The CS time (t_{CS}) is related to L_{ref} via $t_{CS} = L_{ref}/2c$, where $L_{ref} = 30\lambda$ and c is the light speed. The t_{CS} value was $15T_0$ in the E-FPM case, which denotes that E-FPM kept the reflected pulse focused during the entire CS process, thus guaranteeing highly efficient CS.

Figure 5 illustrates the temporal evolutions of the electron energy and the radiated photon beam quality during the scattering process under the three cases. The left column depicts that as the collision process progressed, the electrons transferred energy to the radiated photons, which decreased the electron energy (E_e) and increased the photon energy (E_p) until they both stabilized, marking the end of the CS process. Furthermore, the right column shows that as the collision process advanced, increasing number of photons were generated, leading to a sharp increase in the photon yield (N_p) until it stabilized at the end of the CS process. During the scattering process, due to the transverse force exerted by the laser on the electrons, the radiated photons acquired a certain emittance. Consequently, the divergence angle of the photons (θ_p) increased until the end of the CS process, whereupon the divergence angle stabilized.

Moreover, approximately 7, 9, and 13μJ electron energies were transported to the emitted radiations through CS in the PPM, P-FPM, and E-FPM cases, respectively, as shown in the left column figures in Fig. 5. This implies that the laser utilization efficiency of E-FPM was higher by 86% and 44% compared to that of PPM and P-FPM, respectively. This can be attributed to the boosted L_{ref} and a_0 of E-FPM. Compared to PPM and P-FPM, since the radiation energy of E-FPM was boosted, as shown in Figs. 5(d)–5(f), the photon number and collimation of the emitted radiation of E-FPM were also improved. Specifically, E-FPM increased the photon number of the emitted ray to approximately 12×10^7, an increase in 50% and 70% compared to PPM and P-FPM, respectively. Additionally, E-FPM decreased the average emission angle of the emitted photons to $1.8 \times 10^{-2^\circ}$, which was 3/5 and 3/25 of that afforded by PPM and P-FPM, respectively. While P-FPM improved the radiation energy compared to PPM, its boosted transverse electric field of the reflected pulse stemming from the ultra-tight focusing effect degraded the collimation of the radiated photons.

The enhanced a_0 by P-FPM or E-FPM arising from the refocusing effect could improve the energy and photon number in the radiation beam. This is attributed to the enhanced radiation reaction force and photon number density of the reflected laser resulting from the increase in the reflected a_0. First, the radiation reaction force[70] is scaled by a_0 as $f_{RR} \sim 4\pi\alpha\hbar\omega_L\gamma_0^2 a_0^2/(3\lambda)$, indicating that the radiation recoil force increases with the a_0 value. Thus, the enhanced a_0 after reflection by P-FPM or E-FPM augmented the radiation recoil force, thereby improving the radiation energy. Second, a_0^2 is proportional to the density of the laser photon number (n_γ): $a_0^2 = \frac{\hbar e^2}{m_e^2 c^2 \omega_L} n_\gamma = 4\pi\alpha\nu^2\lambda^3 n_\gamma$, where $\nu \equiv \hbar\omega_L/m_e c^2$ is the normalized laser frequency; $\lambda^3 n_\gamma$ is the number of laser photons in a cube with side λ; $\hbar$ is the Dirac constant; e is the unit charge; m_e is the electron mass; and ω_L is the laser frequency. The probability of multiphoton scattering $e^- + n\gamma_L \rightarrow e^- + \gamma$ (where n is the number of laser photons participating the in multiphoton scattering) is proportional to the laser photon density, that is, proportional to the scattering laser intensity: $n_\gamma^n \sim a_0^{2n}$. Thus, the enlarged scattering laser intensity improved the probability of multiphoton scattering, thereby boosting the number of CS photons.

After CS, 0.5, 0.7, and 0.7 MeV photon beams were obtained in PPM, P-FPM, and E-FPM cases, respectively, as shown in Fig. 6. In the E-FPM case, the energy spread of the emitted photon bunch was 20%, which was 1/2 that of the P-FPM case, and the angular spread was less than 0.02°, which was only 1/28 that of the P-FPM case and

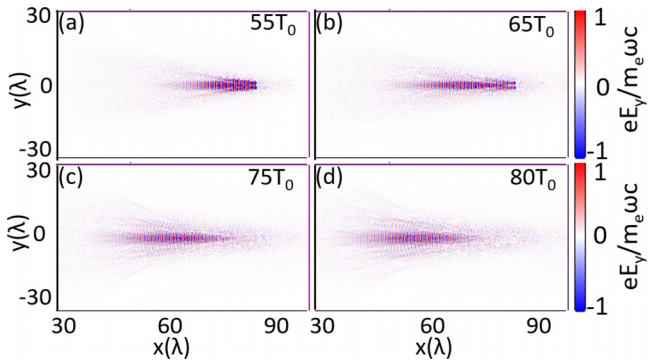

FIG. 4. Electric field distributions of the laser reflected by E-FPM at (a) $55T_0$, (b) $65T_0$, (c) $75T_0$, and (d) $85T_0$.

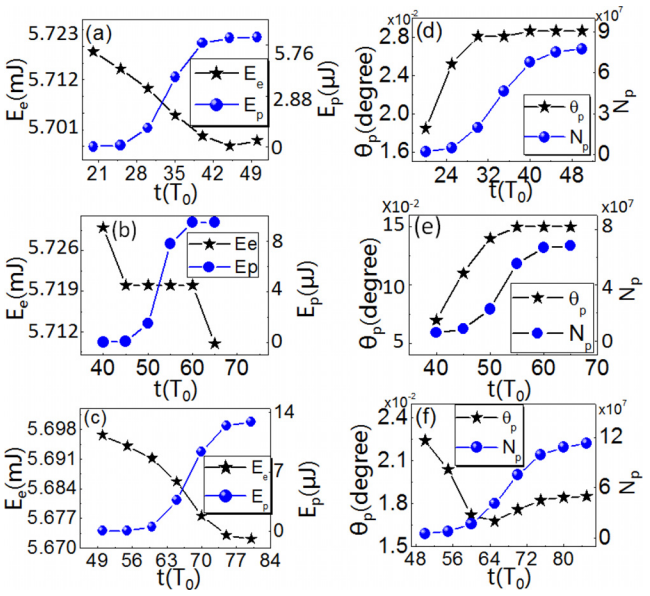

FIG. 5. Time evolutions of the electron energy (E_e) and radiated photon energy (E_p) in the (a) PPM, (b) P-FPM, and (c) E-FPM cases. (d)–(f) Corresponding time evolutions of the average emission angle (θ_p) and emitted photon number (N_p) in the three cases.

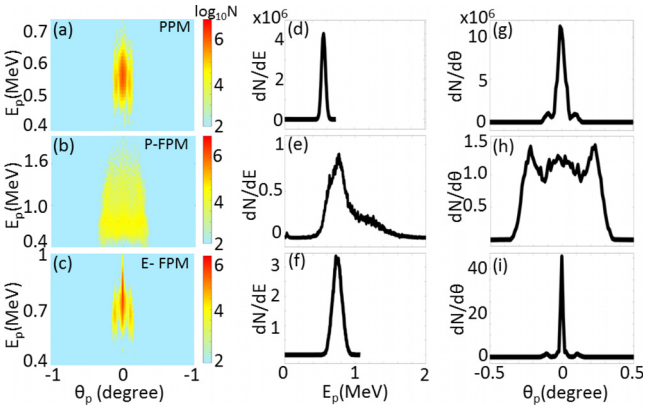

FIG. 6. (a)–(c) Energy–angular distribution, (d)–(f) energy spectra, and (g)–(i) angular spectra of the radiated photons in the PPM, P-FPM, and E-FPM cases, respectively.

1/3 that of the PPM case. In terms of the energy–angle distribution, the photon distribution afforded in the E-FPM case was more compact than that afforded by the other two cases.

During the realization of CS with laser–electron beam collisions, the electron beam energy distribution plays a crucial role in determining the spectral distribution of the resulting photon beam. A non-monoenergetic electron beam yields a broad spectrum of the produced photon beam. However, the study simulations employed an electron beam generated by an LWFA, which is notably characterized by its monoenergetic properties. The use of such electron beams for CS results in photon beams that exhibit high monochromaticity. This has been effectively demonstrated by Yu *et al.*[65] In Yu *et al.*, the head-on collision of an LWFA-produced a monoenergetic electron beam with a laser yielded γ-rays in the MeV range with excellent monochromaticity—approximately 30%, with energy typically ranging from 20% to 40% in the structured plasma mirror cases. The simulation and experimental results of Yu *et al.* confirmed the monochromatic nature of Compton photon beams produced through LWFAs. Conversely, electron beams from other types of acceleration mechanisms tend to exhibit reduced monoenergetic qualities, which decreases the monochromaticity of the resultant γ-rays. Hence, LWFA-produced electron beams were employed in the CS analyses herein.

III. VERIFICATION OF IMPACT OF EXTENDING REFLECTED PULSE LENGTH ON CS BY PARAMETER SCANNING

The above discussion showed that the CS efficiency can be improved by increasing the reflected a_0. Both P-FPM and E-FPM can boost the reflected a_0, but P-FPM yields slightly higher reflected a_0 than E-FPM. However, compared to P-FPM, E-FPM boosts the CS efficiency, which is attributed to the boosted L_{ref} in the latter case. This study verified this inference through multiple sets of numerical simulations. In each simulation set, a crucial parameter, including the reflected a_0, focal length of reflected laser, or delay between the electrons and driving laser, was maintained constant. Table I illustrates the simulation results, showing that when any one of the aforementioned parameters was kept constant, E-FPM still substantially enhanced the CS efficiency compared to P-FPM. This eliminated the possibility of scattering improvement stemming from the aforementioned parameters. When the increase in L_{ref} was weak, E-FPM did not exhibit an advantage in terms of CS efficiency compared to P-FPM. These simulation results further demonstrate that the CS efficiency increases with L_{ref}.

IV. DISCUSSION ON THE IMPACT OF VARIOUS ADVERSE EXPERIMENTAL FACTORS ON THESE THREE SCATTERING SCHEMES

Considering the complexities of real-world experiments, the impact of non-ideal conditions on various scattering mechanisms need to be assessed. The following non-ideal conditions were considered: (1) misalignment between the beams and structured target axis, (2) reduction in the driving laser pulse length from the laser depletion during wakefield acceleration, and (3) presence of pre-plasma from the reflection mirrors. Through a series of comparative simulations, this study explored how the beam–target offset distance, driving laser pulse length, and mirror pre-plasma size influence the scattering results. Tables II–IV depict the effects of these parameters on the scattering outcomes under the different schemes.

The tables show that the scattering efficiency diminished regardless of the type of mirror structure used under the three non-ideal conditions. Furthermore, as these parameters increased, the degradation in scattering efficiency became more pronounced. However, under these non-ideal conditions, E-FPM still exhibited advantages in terms of the CS efficiency relative to both P-FPM and PPM. These comparative results highlight the robustness of E-FPM under less-than-ideal experimental conditions and its potential superiority in enhancing the CS efficiency in practical applications.

TABLE I. Photon number (N_p), total energy (E_p), peak energy (E_{peak}), and energy spread ($\Delta E/E$) of the emitted beams for five comparative cases. Case I, as a reference case, employed P-FPM with $k_1 = 17$. Cases II–V employed E-FPMs with the following parameters: Case II: $k_2 = 0.045$, $c_0 = x_1 = 86\lambda$, and $y_0 = 3\lambda$; Case III: $k_2 = 0.06$, $c_0 = 85\lambda$, $x_1 = 86\lambda$, and $y_0 = 3\lambda$; Case IV: $k_2 = 0.03$, $c_0 = x_1 = 86\lambda$, and $y_0 = 3\lambda$; and Case V: $k_2 = 0.2$, $c_0 = x_1 = 86\lambda$, and $y_0 = -2\lambda$. The parameters were selected to ensure that compared to case I, the reflected a_o in case II, the focal length of the reflected pulse in case III, and the delay distance between electrons and driving laser in case IV remained constant. Moreover, the increase in the effective L_{ref} of the reflected laser was weak in case V.

		N_p (10^7)	E_p (μJ)	E_{peak} (MeV)	$\Delta E/E$ (%)
Case I	Reference case	8	12	0.8	48
Case II	Same laser intensity after reflection compared with case I	11.2	16	1.0	31
Case III	Same focal length compared with case I	12.2	19	1.2	23
Case IV	Same delay between the electron bunch and laser compared with case I	11.2	18	1.0	28
Case V	Increase in effective duration is weak	5.74	4	0.45	48

TABLE II. Total photon energy (E_p) radiated in the P-FPM and E-FPM cases under various lateral beam-mirror offset conditions (D_{offset}).

	$D_{offset}=0$ $E_p(\mu J)$	$D_{offset}=1$ λ $E_p(\mu J)$	$D_{offset}=5$ λ $E_p(\mu J)$	$D_{offset}=8$ λ $E_p(\mu J)$
P-FPM	9.6	7.3	0.91	0.37
E-FPM	12.9	9.6	1.1	0.72

TABLE III. Photon energy output (E_p) in the PPM, P-FPM, and E-FPM cases under various laser pulse lengths (L).

	$L=15\lambda$ $E_p(\mu J)$	$L=12\lambda$ $E_p(\mu J)$	$L=8\lambda$ $E_p(\mu J)$
PPM	6.9	5.5	3.5
P-FPM	9.6	8.5	5.6
E-FPM	12.9	10.3	6.7

TABLE IV. Photon energy output (E_p) in the PPM, P-FPM, and E-FPM cases under various preplasma lengths (L_{pre}).

	$L_{pre}=0$ E_p (μJ)	$L_{pre}=0.5\lambda$ E_p (μJ)	$L_{pre}=1\lambda$ E_p (μJ)
PPM	6.9	6.8	6.7
P-FPM	9.6	9	7.5
E-FPM	12.9	12.4	11.3

V. IMPACT OF THE E-FPM CONFIGURATION ON THE REFLECTED LASER PROFILE AND SCATTERING RESULTS

A. Scaling law of the pulse length and radius of the reflected laser with E-FPM configuration

Equation (2) provides the dependence of L_{ref} on the plasma mirror parameters, indicating that in the E-FPM case, L_{ref} is determined by the parameter k_2. To validate this dependence, two simulation cases are investigated with $k_2 = 0.06$, and 0.1. Under these two cases, the theoretical values of L_{ref} were 33λ and 23λ and the simulation values were 30λ and 20λ, respectively, as shown in Figs. 7(a) and 7(b). This

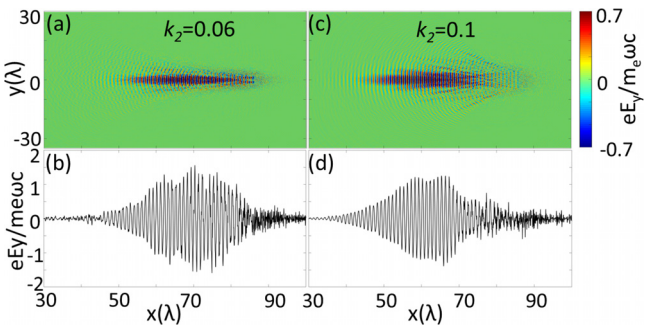

FIG. 7. Profiles of the reflected lasers in the (a) $k_2 = 0.06$ and (c) $k_2 = 0.1$ cases. (b) and (d) Transverse electric field distributions of the reflected pulses along $y = 0$ for the cases depicted in (a) and (c), respectively.

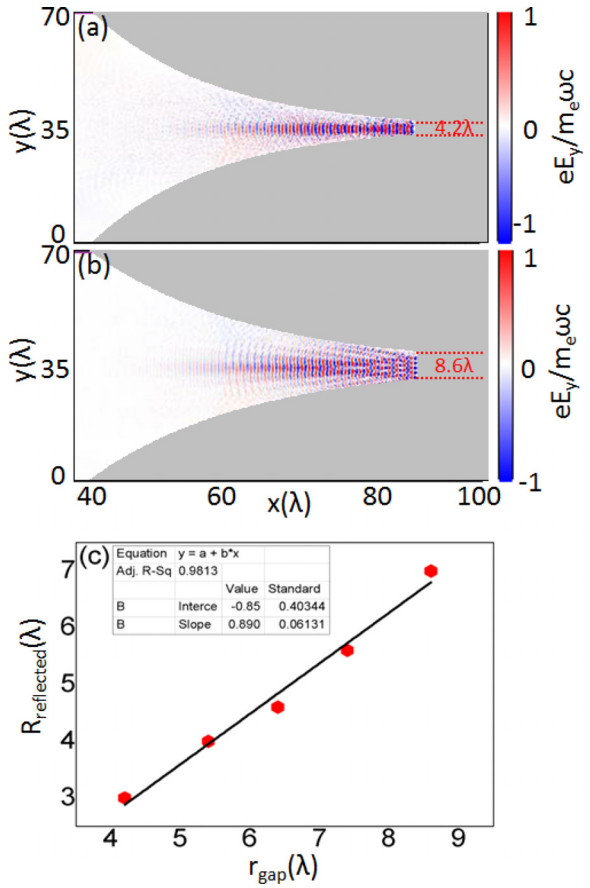

FIG. 8. Outlines of the reflection mirrors and reflected pulses with (a) $r_{gap} = 4.2\lambda$ and (b) $r_{gap} = 8.6\lambda$. (c) Dependence of the reflected laser spot radius on the plasma mirror parameter r_{gap}, with the linear fitting results.

shows that the theoretical predictions and simulation results well matched, demonstrating the reliability of the theoretical predictions and proving that L_{ref} varied with k_2.

Analysis also demonstrated that the reflected laser radius (R_{ref}) was influenced by the E-FPM parameter r_{gap} [as marked in Figs. 2(c) and 3(c)]. R_{ref} increased with r_{gap} from 4.2λ to 8.6λ, as presented in Figs. 8(a) and 8(b). Moreover, the dependence of R_{ref} on r_{gap} can be represented as $R_{ref} = k_0 r_{gap}$. Through five more simulations and the linear fitting of these numerical results, as shown in Fig. 8(c), $k_0 = 0.89$ was obtained. Therefore, R_{ref} is related to r_{gap} as

$$R_{ref} = 0.89 r_{gap}. \quad (3)$$

By exploiting Eqs. (2) and (3), the pulse length and radius of the reflected laser can be adjusted to modulate its profile in the E-FPM case.

B. Dependence of the scattering effect on parameter k_2

The E-FPM configuration influences the reflected laser shape, thereby impacting the scattering efficiency. Therefore, the dependence of the scattering efficiency on the E-FPM configuration parameters

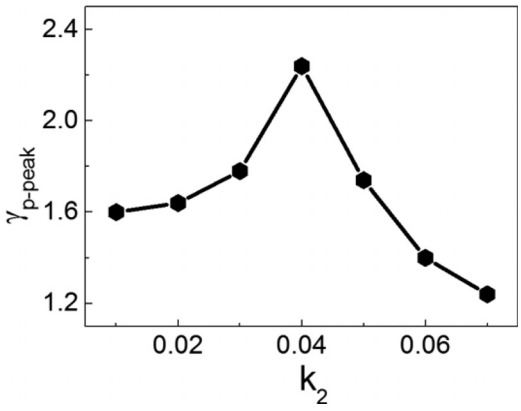

FIG. 9. Dependence of the peak energy (γ_{p-peak}) of emitted photon beams on the E-FPM configuration parameter k_2.

needs to be studied, primarily k_2. By performing more simulations, this section investigated the dependence of the scattering effect on k_2, and Fig. 9 presents the results. The figure shows that for the peak energy of the radiated photons, under our simulation framework, the optimal k_2 value is $k_2 = 0.04$, whereupon the peak energy of the radiated photons (γ_{p-peak}) is 2.24. This represents a 60% increase compared to the $\gamma_{p-peak} = 1.4$ obtained with $k_2 = 0.06$ as used earlier. Additionally, k_2 values ranging from 0.01 to 0.06 can yield radiated photons with $\gamma_{p-peak} \geq 1.4$, demonstrating the robustness of the E-FPM reflection mechanism.

VI. OPTIMAL LWFA PLASMA DENSITY FOR A GIVEN E-FPM CONFIGURATION

For a given E-FPM configuration, an optimal spatial range exists where the reflected laser exhibits excellent focus and high intensity, which is referred to as the focal position range. Before the reflected laser reaches or after it passes this focal position range, the laser is in a divergent state with lower intensity. Thus, the electron and reflected laser were designed to collide within this focal position range as the reflected laser is well-focused and intense in this range, ensuring high scattering efficiency and good quality of the radiated γ-ray beam.

The collision position is determined by the pre-collision electron–laser delay distance d_{e-l}. The colliding electrons typically stem from the LWFA mechanism. For the LWFA electrons, d_{e-l} is determined by the plasma wavelength, which is proportional to the plasma density. Therefore, for the LWFA electrons, the collision position is determined based on the plasma density. However, the focal position is determined according to the E-FPM configuration. To align the collision position with the focal position, the LWFA plasma density needs to be matched with the E-FPM configuration. In other words, for a given E-FPM configuration, an optimal LWFA plasma density exists.

Within this optimal density range, collisions occur at the focal position of the reflected laser, leading to high scattering efficiency and good quality of the photon beam. Outside this optimal density range, electrons collide with the divergent weaker laser, resulting in poor collision effects. Herein, through theoretical analysis, the optimal LWFA gas density for a given set of E-FPM configuration parameters was determined.

For single-pulse CS, d_{e-l} is a key factor affecting the scattering location. When the collision occurs at the center of the focused reflected laser, d_{e-l} and d_{l-m} should fulfill the following condition: $d_{e-l} = 2d_{l-m}$. Here, d_{l-m} is the distance between the center of the focused reflected laser and the mirror and is determined by the mirror configuration. In the E-FPM cases, the theoretical optimal value for d_{e-l} was 33λ, which is consistent with the corresponding simulation value of 32.5λ. Single-pulse CS typically relies on the LWFA mechanism, where d_{e-l} is typically half the plasma wavelength, i.e., $d_{e-l} = \frac{1}{2}\lambda_p$, and λ_p depends on the LWFA plasma density. Therefore, to obtain the optimal d_{e-l}, the optimal LWFA plasma density needs to be employed. Under this optimal condition, the scaling law $d_{e-l} = \frac{1}{2}\lambda_p = 2d_{l-m}$ should be satisfied. Upon substituting the expression for λ_p into this equation, where $\lambda_p(\mu m) = \lambda(\mu m)\sqrt{n_c/n_e}$ and $\lambda(\mu m)\sqrt{a_0 n_c/n_e}/\pi$ in the linear and nonlinear regimes, respectively, the optimal plasma density for LWFA was theoretically derived:

$$n_{LWFA-1} = \begin{cases} \dfrac{n_c\lambda^2}{16\pi^2\left[\dfrac{lnR}{k_2} + R\cdot\tan\left(2\theta_2 - \dfrac{\pi}{2}\right)\right]^2}, \\ \text{for the linear E-FPM regime} \\ \dfrac{a_0 n_c\lambda^2}{16\pi^4\left[\dfrac{lnR}{k_2} + R\cdot\tan\left(2\theta_2 - \dfrac{\pi}{2}\right)\right]^2}, \\ \text{for the non linear E-FPM regime.} \end{cases} \quad (4)$$

For the E-FPM case, as the reflection pulse was able to maintain the focusing shape for a long time, when the CS occurred at the leading edge of the reflected laser, the scattering effect was considerable. In this case, $2d_{l-m} + \frac{1}{2}L_{ref} = \frac{1}{2}\lambda_p$. Therefore, the density for LWFA in this case was

$$n_{LWFA-2} = \begin{cases} \dfrac{n_c\lambda^2}{36\pi^2\left[\dfrac{lnR}{k_2} + R\cdot\tan\left(2\theta_2 - \dfrac{\pi}{2}\right)\right]^2}, \\ \text{for the linear E-FPM regime} \\ \dfrac{a_0 n_c\lambda^2}{36\pi^4\left[\dfrac{lnR}{k_2} + R\cdot\tan\left(2\theta_2 - \dfrac{\pi}{2}\right)\right]^2}, \\ \text{for the non linear E-FPM regime.} \end{cases} \quad (5)$$

Thus, the density range of LWFAs for high-efficiency scattering in E-FPM cases is $n_{LWFA-2} < n_e < n_{LWFA-1}$. The Appendix provides a detailed discussion of the above process.

VII. CONCLUSION

To implement single-pulse CS, plasma mirrors of various shapes are often employed. A planar mirror is often the first choice owing to its less stringent experimental condition requirements and the robustness of the scattering results. However, planar mirrors typically result in low radiation energy and laser utilization. A common alternative is the concave focusing mirror, which increases the reflected laser intensity via focusing, thereby increasing the radiation energy. However, disadvantageously, in some cases, the transverse and longitudinal sizes

of the reflected laser might be very small, which reduces the collision area with the electrons and the scattering time. Moreover, ultra-tight focused reflected lasers weaken the collimation of the radiation photon beam. The proposed convex plasma mirror can focus the reflected laser, which increases its intensity and pulse length, consequently enhancing the scattering time. Furthermore, the planar part at the bottom can be used to adjust the reflected laser radius, allowing it to transversely fully cover the colliding electron beam at the collision point without reducing the scattering area. The impact of these three mirrors on CS was compared through numerical simulations and theoretical analyses. The simulation results confirmed the advantages and disadvantages of these three mirrors, highlighting the advantages of the proposed mirror. The gas density range of the LWFA, required for realizing high-efficiency CS, was also determined.

In this paper, we improve the scattering efficiency and the quality of the radiation photon beam by shaping the colliding laser in Compton scattering to match the configuration of the colliding electron beam. In single-pulse Compton scattering, besides modulating the reflected laser, the quality of the radiated photon beam can also be improved by Yu *et al.*[62,71] enhancing the quality of the electron beam. When the electron beam quality is sufficiently high, other novel mechanisms, in addition to Compton scattering, can also produce high-quality photon beams. For example, Zhu *et al.*[72] successfully obtained a highly bright GeV γ-ray beam through a two-stage laser-plasma interaction. The first stage produces an electron beam, and the second stage generates the photon beam. A crucial reason for achieving such high-energy, high-brightness photon beams in the second stage is that the wakefield acceleration in the first stage provides a high-charge (tens of nC), high-energy (multi-GeV) electron beam. Such a high-quality electron beam sets the conditions for generating high-brightness, high-energy photon beams. Therefore, in our next steps, we will focus on how to apply improved electron acceleration mechanisms to our proposed scheme. For instance, combine the electron acceleration scheme from the work of Zhu *et al.*[72] with our proposed reflector.

ACKNOWLEDGMENTS

This work was supported by the Natural Science Foundation of China under Contract No. 11804348.

AUTHOR DECLARATIONS

Conflict of Interest

The authors have no conflicts to disclose.

Author Contributions

Qin Yu: Conceptualization (equal); Investigation (equal); Software (equal); Validation (equal); Visualization (equal); Writing – original draft (equal); Writing – review & editing (equal). **Yanjun Gu:** Conceptualization (equal); Investigation (equal); Software (equal); Validation (equal); Visualization (equal). **Yi Zhang:** Conceptualization (equal); Investigation (equal); Project administration (equal); Resources (equal); Software (equal); Supervision (equal); Visualization (equal); Writing – review & editing (equal). **Qing Kong:** Conceptualization (equal); Resources (equal); Supervision (equal); Validation (equal); Writing – review & editing (equal). **Shigeo Kawata:** Conceptualization (equal); Writing – review & editing (equal).

DATA AVAILABILITY

The data that support the findings of this study are available from the corresponding author upon reasonable request.

APPENDIX: LWFA PLASMA DENSITY WHEN THE COLLISION OCCURS WITHIN THE OPTIMAL POSITION RANGE

When the laser–electron collision occurs in the region from the center to the leading edge of the focused reflected laser, the CS efficiency is high and the emitted γ-ray beam quality is optimal. In this section, for E-FPM, the plasma density range for LWFA to achieve efficient CS is theoretically derived, ensuring that the collision occurs in the region from the center to the leading edge of the focused reflected laser.

Based on the E-FPM shape and using geometric optics, the pulse length of the reflected laser is

$$L_{ref} = \frac{\ln \mathrm{R}}{k_2} + \mathrm{R} \cdot \tan\left(2\theta_2 - \frac{\pi}{2}\right), \tag{A1}$$

where $\theta_2 = \arctan(k_2 \cdot R)$. Based on the shape evolution of the reflected laser in simulations, the distance from the center point of the focused reflected laser to the plasma mirror d_{l-m} is as follows:

$$d_{l-m} = \frac{1}{2} L_{ref} = \frac{\ln \mathrm{R}}{2k_2} + \frac{1}{2}\mathrm{R} \cdot \tan\left(2\theta_2 - \frac{\pi}{2}\right). \tag{A2}$$

For the electrons to collide with the center of the reflected laser, the distance d_{e-l} between the electrons and driving laser before the collision should be

$$d_{\mathrm{e}-l} = 2d_{l-m} = \frac{\ln \mathrm{R}}{k_2} + \mathrm{R} \cdot \tan\left(2\theta_2 - \frac{\pi}{2}\right). \tag{A3}$$

In the LWFA mechanism, at the end of the acceleration, the accelerated electrons are positioned at the center of the plasma wave. Here, the distance between the accelerated electrons and driving laser is

$$d_{\mathrm{e}-l} = \frac{1}{2}\lambda_p, \tag{A4}$$

where λ_p is the plasma wavelength. For electrons from LWFA to collide with the focused reflected laser at its center, d_{e-l} must satisfy both Eqs. (A3) and (A4). Thus,

$$\lambda_p = 2d_{\mathrm{e}-l} = 4d_{l-m} = 2\frac{\ln \mathrm{R}}{k_2} + 2\mathrm{R} \cdot \tan\left(2\theta_2 - \frac{\pi}{2}\right). \tag{A5}$$

If the driving laser of the plasma wave has non-relativistic intensity, the plasma wavelength is directly determined by the plasma density:

$$\lambda_{\mathrm{p}}(\mu\mathrm{m}) = \lambda(\mu\mathrm{m})\sqrt{n_{\mathrm{c}}/n_{\mathrm{e}}}. \tag{A6}$$

If the driving laser reaches relativistic intensities, the plasma wavelength needs to be relativistically corrected:

$$\lambda_{\mathrm{p}}(\mu\mathrm{m}) = \lambda(\mu\mathrm{m})\sqrt{a_0 n_{\mathrm{c}}/n_{\mathrm{e}}}/\pi. \tag{A7}$$

Substitution of Eqs. (A6) and (A7) into Eq. (A5) yields the LWFA plasma density required for the collision of electrons with the focused reflected laser at the laser's center:

$$n_{\mathrm{LWFA}-1}=\begin{cases}\dfrac{n_c\lambda^2}{16\pi^2\left[\dfrac{lnR}{k_2}+R\cdot\tan\left(2\theta_2-\dfrac{\pi}{2}\right)\right]^2}, \\ \text{for the linear E-FPM regime} \\ \dfrac{a_0 n_c\lambda^2}{16\pi^4\left[\dfrac{lnR}{k_2}+R\cdot\tan\left(2\theta_2-\dfrac{\pi}{2}\right)\right]^2}, \\ \text{for the non linear E-FPM regime.}\end{cases} \tag{A8}$$

Since the laser reflected by E-FPM can maintain a focused state for a long time, collisions occurring at the leading edge of the reflected laser can also ensure good scattering effects. When the collision occurs at the leading edge of the reflected laser, Eq. (A3) should be revised to

$$\mathrm{d}_{e-l}=3d_{l-m}=\frac{\mathrm{lnR}}{k_2}+\mathrm{R}\cdot\tan\left(2\theta_2-\frac{\pi}{2}\right). \tag{A9}$$

Substitution of Eq. (A9) into Eq. (A4) yields

$$\lambda_p=2d_{e-l}=6d_{l-m}=3\frac{\mathrm{lnR}}{k_2}+3\mathrm{R}\cdot\tan\left(2\theta_2-\frac{\pi}{2}\right). \tag{A10}$$

Substituting Eqs. (A6) and (A7) into Eq. (A10), the LWFA plasma density when the collision occurs at the leading edge of the focused reflected laser is obtained:

$$n_{\mathrm{LWFA}-2}=\begin{cases}\dfrac{n_c\lambda^2}{36\pi^2\left[\dfrac{lnR}{k_2}+R\cdot\tan\left(2\theta_2-\dfrac{\pi}{2}\right)\right]^2}, \\ \text{for the linear E-FPM regime} \\ \dfrac{a_0 n_c\lambda^2}{36\pi^4\left[\dfrac{lnR}{k_2}+R\cdot\tan\left(2\theta_2-\dfrac{\pi}{2}\right)\right]^2}, \\ \text{for the non linear E-FPM regime.}\end{cases} \tag{A11}$$

When the collision occurs at any point from the leading edge to the center of the focused reflected laser, the scattering exhibits relatively high efficiency. Therefore, for high-efficiency CS, the LWFA plasma density n_{LWFA} must satisfy

$$n_{\mathrm{LWFA}-2}< n_{\mathrm{LWFA}}< n_{\mathrm{LWFA}-1}. \tag{A12}$$

Equation (A12) presents the LWFA plasma density range for achieving efficient CS.

REFERENCES

[1]M. Litos, E. Adli, W. An, C. I. Clarke, C. E. Clayton, S. Corde, J. P. Delahaye, R. J. England, A. S. Fisher, J. Frederico *et al.*, Nature **515**, 92–95 (2014).
[2]J. Faure, Y. Glinec, A. Pukhov, S. Kiselev, S. Gordienko, E. Lefebvre, J.-P. Rousseau, F. Burgy, and V. Malka, Nature **431**, 541–544 (2004).
[3]S. P. Mangles, C. D. Murphy, Z. Najmudin, A. G. R. Thomas, J. L. Collier, A. E. Dangor, E. J. Divall, P. S. Foster, J. G. Gallacher, C. J. Hooker *et al.*, Nature **431**, 535–538 (2004).
[4]C. Geddes, C. Toth, J. van Tilborg, E. Esarey, C. B. Schroeder, D. Bruhwiler, C. Nieter, J. Cary, and W. P. Leemans, Nature **431**, 538–541 (2004).
[5]W. P. Leemans, B. Nagler, A. J. Gonsalves, C. Toth, K. Nakamura, C. G. R. Geddes, E. Esarey, C. B. Schroeder, and S. M. Hooker, Nat. Phys. **2**, 696–699 (2006).
[6]J. Faure, C. Rechatin, A. Norlin, A. Lifschitz, Y. Glinec, and V. Malka, Nature **444**, 737–739 (2006).
[7]W. Lu, M. Tzoufras, C. Joshi, F. S. Tsung, W. B. Mori, J. Vieira, R. A. Fonseca, and L. O. Silva, Phys. Rev. ST Accel. Beams **10**, 061301 (2007).
[8]V. Malka, S. Fritzler, E. Lefebvre, M.-M. Aleonard, F. Burgy, J.-P. Chambaret, J.-F. Chemin, K. Krushelnick, G. Malka, S. P. D. Mangles *et al.*, Science **298**, 1596–1600 (2002).
[9]N. A. Hafz, T. M. Jeong, I. W. Choi, S. K. Lee, K. H. Pae, V. V. Kulagin, J. H. Sung, T. J. Yu, K.-H. Hong, T. Hosokai *et al.*, Nat. Photonics **2**, 571–577 (2008).
[10]S. W. Wilkins, T. E. Gureyev, D. Gao, A. Pogany, and A. Stevenson, Nature **384**, 335–338 (1996).
[11]S. Chen, G. Golovin, C. Miller, D. Haden, S. Banerjee, P. Zhang, C. Liu, J. Zhang, B. Zhao, S. Clarke *et al.*, Nucl. Inst. Methods Phys. Res. B **366**, 217–223 (2016).
[12]J. C. Wood, D. J. Chapman, K. Poder, N. C. Lopes, M. E. Rutherford, T. G. White, F. Albert, K. T. Behm, N. Booth, J. S. J. Bryant *et al.*, Sci. Rep. **8**, 11010 (2018).
[13]B. Girolami, B. Larsson, M. Preger, C. Schaerf, and J. Stepanek, Phys. Med. Biol. **41**, 1581 (1996).
[14]K. Sakaue, A. Endo, and M. Washio, J. Micro/Nanolithogr. MEMS MOEMS **11**, 021124 (2012).
[15]F. Albert, S. G. Anderson, D. J. Gibson, R. A. Marsh, S. S. Wu, C. W. Siders, C. P. J. Barty, and F. V. Hartemann, Phys. Rev. ST Accel. Beams **14**, 050703 (2011).
[16]E. Kwan, G. Rusev, A. S. Adekola, F. Donau, S. L. Hammond, C. R. Howell, H. J. Karwowski, J. H. Kelley, R. S. Pedroni, R. Raut *et al.*, Phys. Rev. C **83**, 041601 (2011).
[17]U. Kneissl, H. Pitzang, and A. Zilges, Prog. Part. Nucl. Phys. **37**, 349–433 (1996).
[18]X. Wang, Z. Xu, W. Luo, H. Lu, Z. Zhu, and X. Yan, Phys. Plasmas **24**, 093105 (2017).
[19]E. Irani, H. Omidvar, and R. Sadighi-Bonabi, Energy Convers. Manage. **77**, 558–563 (2014).
[20]H. Lan, T. Song, Z. Luo, J. Zhou, Z. Zhu, and W. Luo, Phys. Rev. Appl. **16**, 054048 (2021).
[21]R. Hajima, N. Kikuzawa, N. Nishimori, T. Hayakawa, T. Shizuma, K. Kawase, M. Kando, E. Minehara, H. Toyokawa, and H. Ohgaki, Nucl. Instrum. Methods A **608**, S57 (2009).
[22]W. Luo, Nucl. Sci. Technol. **27**, 96 (2016).
[23]H.-Y. Lan, T. Song, J.-L. Zhang, J.-L. Zhou, and W. Luo, Nucl. Sci. Technol. **32**, 84 (2021).
[24]V. Tomkus, V. Girdauskas, J. Dudutis, P. Gečys, V. Stankevič, G. Račiukaitis, I. G. González, D. Guénot, J. B. Svensson, A. Persson *et al.*, Sci. Rep. **10**, 16807 (2020).
[25]C. Brady, C. Ridgers, T. Arber, and A. Bell, Phys. Plasmas **21**, 033108 (2014).
[26]D. Wu, W. Yu, Y. Zhao, S. Fritzsche, and X. He, Matter Radiat. Extremes **3**, 293–299 (2018).
[27]M. Chistyakov, D. Rumyantsev, and N. Stus, Phys. Rev. D **86**, 043007 (2012).
[28]F. Mackenroth, N. Kumar, N. Neitz, and C. H. Keitel, Phys. Rev. E **99**, 033205 (2019).
[29]J. Feng, J. Wang, Y. Li, C. Zhu, M. Li, Y. He, D. Li, W. Wang, and L. Chen, Phys. Plasmas **24**, 093110 (2017).
[30]C. Harvey, M. Marklund, and A. R. Holkundkar, Phys. Rev. ST Accel. Beams **19**, 094701 (2016).
[31]B. Shen and J. Meyer-ter-Vehn, Phys. Rev. E **65**, 016405 (2001).
[32]Y. Wu, C. Yu, Z. Qin, W. Wang, R. Qi, Z. Zhang, K. Feng, L. Ke, Y. Chen, C. Wang *et al.*, Plasma Phys. Controlled Fusion **61**, 085030 (2019).
[33]N. D. Powers, I. Ghebregziabher, G. Golovin, C. Liu, S. Chen, S. Banerjee, J. Zhang, and D. P. Umstadter, Nat. Photonics **8**, 28–31 (2014).
[34]W. Leemans, A. J. Gonsalves, H.-S. Mao, K. Nakamura, C. Benedetti, C. B. Schroeder, C. Tóth, J. Daniels, D. E. Mittelberger, S. S. Bulanov *et al.*, Phys. Rev. Lett. **113**, 245002 (2014).
[35]A. Gonsalves, K. Nakamura, J. Daniels, H.-S. Mao, C. Benedetti, C. B. Schroeder, C. Tóth, J. van Tilborg, D. E. Mittelberger, S. S. Bulanov *et al.*, Phys. Plasmas **22**, 056703 (2015).
[36]K. Oubrerie, A. Leblanc, O. Kononenko, R. Lahaye, I. A. Andriyash, J. Gautier, J.-P. Goddet, L. Martelli, A. Tafzi, K. Ta Phuoc *et al.*, Sci. Appl. **11**, 180 (2022).

[37]H. T. Kim, V. B. Pathak, K. Hong Pae, A. Lifschitz, F. Sylla, J. H. Shin, C. Hojbota, S. Ku Lee, J. H. Sung, H. W. Lee *et al.*, Sci. Rep. **7**, 10203 (2017).
[38]T. Long, C. T. Zhou, T. W. Huang, K. Jiang, L. B. Ju, H. Zhang, T. X. Cai, M. Y. Yu, B. Qiao, S. C. Ruan *et al.*, Plasma Phys. Controlled Fusion **61**, 085002 (2019).
[39]T. Brümmer, S. Bohlen, F. Grüner, J. Osterhoff, and K. Põder, Sci. Rep. **12**, 16017 (2022).
[40]J. Vyskočil, E. Gelfer, and O. Klimo, Plasma Phys. Control. Fusion **62**, 064002 (2020).
[41]Z. Gong, R. H. Hu, H. Y. Lu, J. Q. Yu, D. H. Wang, E. G. Fu, C. E. Chen, X. T. He, and X. Q. Yan, Plasma Phys. Controlled Fusion **60**, 044004 (2018).
[42]T. Huang, C. M. Kim, C. T. Zhou, M. H. Cho, K. Nakajima, C. M. Ryu, S. C. Ruan, and C. H. Nam, New J. Phys. **21**, 013008 (2019).
[43]M. Vranic, J. L. Martins, J. Vieira, R. A. Fonseca, and L. O. Silva, Phys. Rev. Lett. **113**, 134801 (2014).
[44]D. Y. Kim, C. Hojbota, M. Mirzaie, S. K. Lee, K. Y. Kim, J. H. Sung, and C. H. Nam, Rev. Sci. Instrum. **93**, 113001 (2022).
[45]Y. Ma, J. Hua, D. Liu, Y. He, T. Zhang, J. Chen, F. Yang, X. Ning, H. Zhang, Y. Du *et al.*, Phys. Rev. Appl. **19**, 014073 (2023).
[46]K. Poder, M. Tamburini, G. Sarri, A. Di Piazza, S. Kuschel, C. D. Baird, K. Behm, S. Bohlen, J. M. Cole, D. J. Corvan *et al.*, Phys. Rev. X **8**, 031004 (2018).
[47]F. Hartemann, D. J. Gibson, W. J. Brown, A. Rousse, K. Ta Phuoc, V. Mallka, and J. Faure, Phys. Rev. ST Accel. Beams **10**, 011301 (2007).
[48]A. Thomas, C. Ridgers, S. Bulanov, B. Griffin, and S. Mangles, Phys. Rev. X **2**, 041004 (2012).
[49]K. Khrennikov, J. Wenz, A. Buck, J. Xu, M. Heigoldt, L. Veisz, and S. Karsch, Phys. Rev. Lett. **114**, 195003 (2015).
[50]C. Zhu, J. Wang, J. Feng, Y. Li, D. Li, M. Li, Y. He, J. Ma, J. Tan, B. Zhang *et al.*, Plasma Phys. Controlled Fusion **61**, 024001 (2019).
[51]A. Döpp, E. Guillaume, C. Thaury, J. Gautier, I. Andriyash, A. Lifschitz, V. Malka, A. Rousse, and K. Ta Phuoc, Plasma Phys. Controlled Fusion **58**, 034005 (2016).
[52]J. P. Palastro, D. Kaganovich, D. Gordon, B. Hafizi, M. Helle, J. Penano, and A. Ting, New J. Phys. **17**, 023072 (2015).
[53]J. Ong, K. Seto, A. Berceanu, S. Aogaki, and L. Neagu, Plasma Phys. Controlled Fusion **61**, 084009 (2019).
[54]K. Ta Phuoc, S. Corde, C. Thaury, V. Malka, A. Tafzi, J. P. Goddet, R. C. Shah, S. Sebban, and A. Rousse, Nat. Photonics **6**, 308–311 (2012).
[55]H.-E. Tsai, X. Wang, J. M. Shaw, Z. Li, A. V. Arefiev, X. Zhang, R. Zgadzaj, W. Henderson, V. Khudik, G. Shvets *et al.*, Phys. Plasma **22**, 023106 (2015).
[56]X.-L. Zhu, M. Chen, T.-P. Yu, S.-M. Weng, L.-X. Hu, P. McKenna, and Z.-M. Sheng, Appl. Phys. Lett. **112**, 174102 (2018).
[57]G. Sarri, D. J. Corvan, W. Schumaker, J. M. Cole, A. Di Piazza, H. Ahmed, C. Harvey, C. H. Keitel, K. Krushelnick, S. P. D. Mangles *et al.*, Phys. Rew. Lett. **113**, 224801 (2014).
[58]S. Corde, K. Ta Phuoc, G. Lambert, R. Fitour, V. Malka, and A. Rousse, Rev. Mod. Phys. **85**, 1 (2013).
[59]G. Z. Sun, E. Ott, Y. Lee, and P. Guzdar, Phys. Fluids **30**, 526–532 (1987).
[60]A. Borisov, A. V. Borovskiy, O. B. Shiryaev, V. V. Korobkin, A. M. Prokhorov, J. C. Solem, T. S. Luk, K. Boyer, and C. K. Rhodes, Phys. Rev. A **45**, 5830 (1992).
[61]W.-M. Wang, Z.-M. Sheng, M. Zeng, Y. Liu, Z.-D. Hu, S. Kawata, C.-Y. Zheng, W. B. Mori, L.-M. Chen, Y.-T. Li *et al.*, Appl. Phys. Lett. **101**, 184104 (2012).
[62]Q. Yu, Y. J. Gu, X. F. Li, S. Huang, F. Zhang, Q. Kong, Y. Y. Ma, and S. Kawata, Phys. Plasma **21**, 113106 (2014).
[63]S. Kashiwagi, M. Washio, T. Kobuki, R. Kuroda, I. Ben-Zvi, I. Pogorelsky, K. Kusche, J. Skaritka, V. Yakimenko, X. J. Wang *et al.*, Nucl. Inst. Methods Phys. Res. A **455**, 36–40 (2000).
[64]I. Pogorelsky, I. Ben-Zvi, T. Hirose, S. Kashiwagi, V. Yakimenko, K. Kusche, P. Siddons, J. Skaritka, T. Kumita, A. Tsunemi *et al.*, Phys. Rev. ST Accel. Beams **3**, 090702 (2000).
[65]C. Yu, R. Qi, W. Wang, J. Liu, W. Li, C. Wang, Z. Zhang, J. Liu, Z. Qin, M. Fang *et al.*, Sci. Rep. **6**, 29518 (2016).
[66]A. Gonsalves, K. Nakamura, C. Lin, D. Panasenko, S. Shiraishi, T. Sokollik, C. Benedetti, C. B. Schroeder, C. G. R. Geddes, J. van Tilborg *et al.*, Nat. Phys. **7**, 862–866 (2011).
[67]S. Banerjee, N. D. Powers, V. Ramanathan, I. Ghebregziabher, K. J. Brown, C. M. Maharjan, S. Chen, A. Beck, E. Lefebvre, S. Y. Kalmykov *et al.*, Phys. Plasmas **19**, 056703 (2012).
[68]E. Brunetti, R. P. Shanks, G. G. Manahan, M. R. Islam, B. Ersfeld, M. P. Anania, S. Cipiccia, R. C. Issac, G. Raj, G. Vieux *et al.*, Phys. Rev. Lett. **105**, 215007 (2010).
[69]A. Pukhov, J. Plasma Phys. **61**, 425–433 (1999).
[70]A. Di Piazza, C. Müller, K. Hatsagortsyan, and C. H. Keitel, Rev. Mod. Phys. **84**, 1177 (2012).
[71]Q. Yu, Q. Kong, Y. Gu, X. Li, S. Huang, and S. Kawata, Europhys. Lett. **110**, 35002 (2015).
[72]X.-L. Zhu, M. Chen, S.-M. Weng, T.-P. Yu, W.-M. Wang, F. He, Z.-M. Sheng, P. McKenna, D. A. Jaroszynski, and J. Zhang, Sci. Adv. **6**, eaaz7240 (2020).